Quantum fluctuations and saturable absorption in mesoscale lasers

Kaushik Roy-Choudhury[1] and A. F. J. Levi[1,2]
[1]*Department of Physics and Astronomy, University of Southern California, Los Angeles, California 90089-0484, USA*
[2]*Department of Electrical Engineering, University of Southern California, Los Angeles, California 90089-2533, USA*
(Received 7 September 2010; published 21 April 2011)

We present a quantum-mechanical treatment of fluctuations and saturable absorption in mesoscale lasers. The time evolution of the density matrix is obtained from numerical integration and field-field and intensity-intensity correlations are calculated to obtain steady-state linewidth and photon statistics. Inclusion of a saturable absorber in the otherwise homogeneous medium is shown to suppress lasing, increase fluctuations, and enhance spontaneous emission near threshold.

DOI: 10.1103/PhysRevA.83.043827 PACS number(s): 42.55.Sa, 42.55.Ah, 42.50.Lc

I. INTRODUCTION

Fluctuations due to quantization can dominate predicted behavior of mesoscale lasers. Using only semiclassical master equations and specific device parameters, it has previously been shown that quantization of particle number, and the fact that a lowest energy state of the system exists, can suppress lasing and enhance spontaneous emission around threshold [1,2]. For this semiclassical system, dynamic switching between two characteristic system states can dominate fluctuations and correlations between n discrete excited electronic emitter states and s discrete photons and create a non-Poisson probability distribution.

However, studying the fundamental contribution of field quantization to noise and fluctuations in mesoscale lasers requires going beyond particle number quantization and semiclassical master equations. Here, we use a quantum-mechanical description of a mesoscale laser containing s cavity photons and N_e emitters and find solutions by direct integration of the system's density matrix. Quantum fluctuations in this finite-sized dissipative system are found to be sensitive to the number of emitters and the presence of inhomogeneous saturable absorption.

This paper is organized as follows. In Sec. II, a model is developed that includes N_e two-level (quantum dot or atom) emitters incoherently pumped by an external reservoir and a quantized photon field with s cavity photons that can decay into an external reservoir through finite reflectivity mirrors. Section III describes the calculated steady-state properties as the number of identical emitters in the cavity is increased. Section IV considers the case of an inhomogeneous active system consisting of identical emitters and a saturable absorber. Under these conditions, the quantum model can predict lasing suppression, enhanced spontaneous emission and the associated emitter excitation number depinning, and bimodal probability distributions. These results allow interpretation of previously reported behavior found by solving the semiclassical master equations [1,2]. Section V describes the predictions of the quantum-model correlation functions for the production of squeezed light.

II. THE MODEL

Figure 1(a) is a schematic diagram of a prototype mesoscale laser consisting of multiple two-level emitters such as quantum dots or atoms coupled to a single-cavity mode in a high-Q optical cavity formed by two partially transmitting mirrors. In our model of this system, both light and emitters are treated quantum mechanically. The number of emitters is N_e and, for simplicity, they are assumed to be in resonance with the single-cavity mode and so detuning is ignored.

As illustrated in Fig. 1(b), emitter electronic states are continuously incoherently pumped at rate P by an external reservoir. The stimulated and spontaneous emission coefficient coupling the ground $|1\rangle$ and excited $|2\rangle$ electronic states of each emitter is g. The separation in emitter eigenenergy is $E_2 - E_1 = \hbar\omega$, where ω is the angular frequency of the high-Q optical cavity resonance. The emitters are damped at rate γ by a reservoir of oscillators representing incoherent decay via spontaneous emission into nonlasing leaky modes. Decay of the laser photon field in the single-cavity mode is by coupling to another external reservoir through partially transmitting mirrors with total loss rate κ.

The Hamiltonian describing two-level emitters coupled to a single-cavity mode and interacting with external reservoirs is

$$H = H_S + H_{RS} + H_R, \tag{1}$$

where H_S is the Hamiltonian of the system of emitters and photons, H_R is the Hamiltonian for the reservoirs, and H_{RS} couples the system to the reservoirs. H_S is the Jaynes-Cummings Hamiltonian [3] coupling a single-cavity mode with the emitters. For a homogeneous system, in which emitter properties are identical,

$$H_S = \omega a^\dagger a + \sum_{k=1}^{N_e} \omega |2_k\rangle\langle 2_k| + g(\sigma_k a^\dagger + a\sigma_k{}^\dagger), \tag{2}$$

where $\hbar = 1$, and the operators $\sigma_k{}^\dagger = |2_k\rangle\langle 1_k|$ and $\sigma_k = |1_k\rangle\langle 2_k|$ couple the ground $|1_k\rangle$ and excited $|2_k\rangle$ electronic states of the emitter k with energies $E_1 = 0$ and $E_2 = \omega$, respectively. The operator $a^\dagger$ creates a photon of energy ω. The coupling terms are evaluated within the dipole and rotating-wave approximation [3].

The Hamiltonian coupling the system to the reservoirs is

$$H_{RS} = \sum_{R''} \mu_{R''}[a b_{R''}^\dagger + b_{R''} a^\dagger] + \sum_R \lambda_R[\sigma_k b_R{}^\dagger + b_R \sigma_k{}^\dagger] + \sum_{R'} \lambda'_{R'}[\sigma_k b_{R'}{}^\dagger + b_{R'} \sigma_k{}^\dagger]. \tag{3}$$

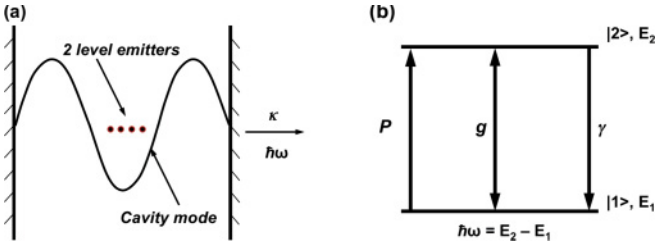

FIG. 1. (Color online) (a) Schematic diagram of multiple emitters coupled to a single optical cavity mode with total mirror loss rate, κ. (b) Processes in a single emitter showing incoherent pump transition rate, P, stimulated and spontaneous coefficient, g, and loss rate, γ. The separation in emitter eigenenergy is $E_2 - E_1 = \hbar\omega$, where ω is the angular frequency of the high-Q optical cavity resonance.

The first term causes direct dissipation of cavity mode photons due to incomplete reflectance of the mirrors and thereby coupling it to the continuum of photonic modes outside the micro-cavity. The second term is dissipation by direct coupling of the emitter to harmonic oscillator photonic modes different from the cavity mode. This describes dissipation of the emitter by spontaneous emission to an external reservoir of photons created by $b_R^\dagger$. The last term is due to the incoherent pump that is modeled as an inverse spontaneous decay process. The pump is a process that couples the emitter with a reservoir of inverted harmonic oscillators [4,5]. The pumping and emission mechanisms in H_{RS} introduce decoherence affecting the quantum properties of the system.

The term H_R describes the external reservoirs of harmonic oscillators with bosonic commutation rules. The coupling constants μ_R and λ_R depend on the particular mode of the reservoir. Detailed derivation of these interactions with reservoirs may be found in Refs. [3,4,6,7].

To describe the different pumping and loss mechanisms for a single emitter it is convenient to work in the basis $(|1s\rangle; |2s\rangle)$, where s is the number of cavity photons and (1, 2) are the states of the emitter. These are product states between the emitter states and the Fock states of the cavity mode. Although the theory may include the effects of finite-temperature reservoirs, we consider the special case of zero temperature ($T = 0$ K) to emphasize the quantum origin of the fluctuations. The reduced density matrix ρ for the coupled emitter-photon system is obtained from the total density matrix ρ_T by tracing out the reservoir degrees of freedom. In the interaction picture for multiple emitters, ρ satisfies the master equation

$$\frac{d\rho}{dt} = \frac{i}{\hbar}[\rho, H_S] + \frac{\kappa}{2}(2a\rho a^\dagger - a^\dagger a\rho - \rho a^\dagger a) + \sum_k \frac{\gamma_k}{2}(2\sigma_k\rho\sigma_k{}^\dagger - \sigma_k{}^\dagger\sigma_k\rho - \rho\sigma_k{}^\dagger\sigma) + \sum_k \frac{P_k}{2}(2\sigma_k{}^\dagger\rho\sigma_k - \sigma_k\sigma_k{}^\dagger\rho - \rho\sigma_k\sigma_k{}^\dagger) \quad (4)$$

or

$$\frac{d\rho}{dt} = \hat{\mathbf{L}}\rho, \quad (5)$$

where $\hat{\mathbf{L}}$ is the time propagator for the density matrix. The master equation is obtained under the Born-Markov approximation [3] for the interaction between the system and the reservoirs. In the chosen basis, the matrix elements of the reduced density operator ρ are

$$\rho_{kn,jm} = \langle kn|\rho|jm\rangle. \quad (6)$$

The diagonal matrix elements describe populations of the emitter-photon levels and the off-diagonal terms quantify the coherence between these levels. Equation (4) may be used to obtain the time evolution of the system. For a single emitter at time $t = 0$ the evolution of the density matrix is

$$\frac{d\rho}{dt} = \begin{bmatrix} \partial_t\rho_{1s,1s} & \partial_t\rho_{1s,2s-1} \\ \partial_t\rho^*_{1s,2s-1} & \partial_t\rho_{2s,2s} \end{bmatrix}, \quad (7)$$

where

$$\partial_t\rho_{1s,1s} = ig\sqrt{s}(\rho_{1s,2s-1} - \rho_{1s-1,2s}) + \gamma\rho_{2s,2s} - \kappa[s\rho_{1s,1s} - (s+1)\rho_{1s+1,1s+1}] - P\rho_{1s,1s}, \quad (8)$$

$$\partial_t\rho_{2s,2s} = ig\sqrt{s+1}(\rho_{1s,2s+1} - \rho_{1s+1,2s}) - \gamma\rho_{2s,2s} - \kappa[s\rho_{2s,2s} - (s+1)\rho_{2s+1,2s+1}] + P\rho_{1s,1s}, \quad (9)$$

$$\partial_t\rho_{1s,2s-1} = ig\sqrt{s}(\rho_{1s,1s} - \rho_{2s-1,2s-1}) - \{[\gamma + \kappa(2s-1) + P]/2\}\rho_{2s,1s-1} + \kappa\sqrt{s(s+1)}\rho_{1s+1,2s}. \quad (10)$$

The interaction parametrized by κ, γ, and P couples matrix elements with different photon occupation number s. This leads to an infinite set of differential equations which are truncated for numerical integration at a high value of s.

The first-order equations derived from the density matrix couples terms in a systematic way. Since there is no detuning, energy units of photons and emitters are the same. The terms $\rho_{1s,1s}$, $\rho_{2s-1,2s-1}$, $\rho_{1s,2s-1}$, and $\rho_{2s-1,1s}$ all have the same units of energy, i.e., s. More importantly, the corresponding bra and ket components of an element have the same energy. For example, $\rho_{1s-1,2s}$ has the same energy of s units for its $\langle 1s-1|$ and $|2s\rangle$. This principle holds for multiple emitters. An example of a density-matrix element of a $N_e = 4$ two-level emitter system is $\langle 2121s|\rho|2221s-1\rangle$, where the first four numbers represent the states of the four emitters. This element is similar to the simple single-emitter element, as it has equal energy in its bra and ket components and also couples with similar equal energy elements. The number of terms coupled grows as 4^{N_e}.

The master equations may be used to compute the dynamics of expectation values of any system operators. The evaluation of the diagonal elements allows calculation of steady-state properties and single time averages of operators. The important photon field-field and intensity-intensity correlations are

$$g^1(t,\tau) = \langle a^\dagger(t)a(t+\tau)\rangle, \quad (11)$$

$$g^2(t,\tau) = \langle a^\dagger(t)a^\dagger(t+\tau)a(t+\tau)a(t)\rangle. \quad (12)$$

In steady state, these correlations do not depend on time t and can be evaluated using

$$\langle a^\dagger(t)a(t+\tau)\rangle = \mathrm{Tr}[ae^{\hat{\mathbf{L}}\tau}(\rho_s a^\dagger)], \quad (13)$$

$$\langle a^\dagger(t)a^\dagger(t+\tau)a(t+\tau)a(t)\rangle = \mathrm{Tr}[a^\dagger ae^{\hat{\mathbf{L}}\tau}(a\rho_s a^\dagger)], \quad (14)$$

which is valid for Markovian systems [4]. Here, ρ_s is the steady-state solution of the master equation (5) and $\hat{\mathbf{L}}$ is the time evolution operator of the density matrix.

The coupled density-matrix equations used to obtain the first-order correlation function $g^1(t,\tau)$ are

$$\partial_t \rho_{1s+1,1s} = ig(\sqrt{s}\rho_{1s+1,2s-1} - \sqrt{s+1}\rho_{2s,1s}) + \gamma\rho_{2s+1,2s} - P\rho_{1s+1,1s} + \frac{\kappa}{2}[2\sqrt{(s+1)(s+2)}\rho_{1s+2,1s+1} - (2s+1)\rho_{1s+1,1s}], \quad (15)$$

$$\partial_t \rho_{2s+1,2s} = ig(\sqrt{s+1}\rho_{2s+1,1s+1} - \sqrt{s+2}\rho_{1s+2,2s}) - \gamma\rho_{2s+1,2s} + P\rho_{1s+1,1s} + \frac{\kappa}{2}[2\sqrt{(s+1)(s+2)} \times \rho_{2s+2,2s+1} - (2s+1)\rho_{2s+1,2s}], \quad (16)$$

$$\partial_t \rho_{2s,1s} = ig(\sqrt{s}\rho_{2s,2s-1} - \sqrt{s+1}\rho_{1s+1,1s}) - [(\gamma + 2s\kappa + P)/2]\rho_{2s,1s} + \kappa(s+1)\rho_{2s+1,1s+1}, \quad (17)$$

$$\partial_t \rho_{1s+1,2s-1} = ig(\sqrt{s}\rho_{1s+1,1s} - \sqrt{s+1}\rho_{2s,2s-1}) - [(\gamma + 2s\kappa + P)/2]\rho_{1s+1,2s-1} + \kappa\sqrt{s(s+2)}\rho_{1s+2,2s}. \quad (18)$$

The terms $\rho_{1s+1,1s}$, $\rho_{2s,2s-1}$, $\rho_{2s,1s}$, and $\rho_{1s+1,2s-1}$ all have the same units of energy, $s+1$ and s, in their bra and ket components, respectively. Similar terms are coupled to each other and the same principle is obeyed when more emitters are added. The steady-state solution to Eqs. (8)–(10) contains terms $\rho_{1s,1s}$, $\rho_{2s-1,2s-1}$, $\rho_{1s,2s-1}$, and $\rho_{2s-1,1s}$. The $a^\dagger$ operator acting on the density matrix produces terms $\rho_{1s+1,1s}$, $\rho_{2s,2s-1}$, $\rho_{2s,1s}$, and $\rho_{1s+1,2s-1}$. Therefore, the steady-state solution to the first set of equations (8)–(10) gives the initial value for the second set of equations (15)–(18). More off-diagonal terms are produced by this operation. The a operator acting on the product of $\rho a^\dagger$ brings back the diagonal, which is then summed to obtain $g^1(t,\tau)$. Likewise, the operation $a\rho a^\dagger$ produces equations coupling terms similar to Eqs. (8)–(10) because of the two operations on the density matrix.

The photon field-field correlation gives information on phase fluctuations and the frequency spectrum of emitted light, $S(\nu)$, may be obtained from the Fourier transform

$$S(\nu) = \frac{1}{\pi}\mathrm{Re}\int_0^\infty d\tau\, e^{i\nu\tau} g^1(t,\tau). \quad (19)$$

The intensity-intensity correlation gives information on photon number statistics. Phenomena such as squeezed states or antibunching may be investigated using this correlation. For zero delay ($\tau = 0$) the normalized second-order correlation obtained from Eq. (14) is

$$G^2(\tau=0) = \frac{\langle a^\dagger a^\dagger a a\rangle}{\langle a^\dagger a\rangle^2} = \frac{\sum_s s(s-1)(\rho_{2s,2s} + \rho_{1s,1s})}{\left[\sum_s s(\rho_{2s,2s} + \rho_{1s,1s})\right]^2}. \quad (20)$$

The Fano factor, or normalized variance, may also be used as a measure of photon number fluctuations and is given by

$$F = \frac{\langle s^2\rangle - \langle s\rangle^2}{\langle s\rangle}, \quad (21)$$

where s is the cavity photon number.

III. SCALING OF LASERS

A. Single emitter

We begin by analyzing the case of a single two-level emitter in a lasing cavity. Figure 2 illustrates the steady-state behavior of a single emitter for different cavity losses as a function of the incoherent pump rate. Parameters used scale within a range corresponding to very recent experiments on single quantum dot [8] and single ion [9] lasers. The cavity with the highest optical Q stores the maximum number of photons and two distinct peaks in the Fano factor are predicted [10]. As shown in Fig. 2(c), the strong photon number fluctuations experienced by the system near lasing threshold pump rates gives rise to a Fano-factor peak at low pump rates. Another peak appears due to self-quenching [10,11] at larger pump rates. This occurs when correlations required for lasing are destroyed by a strong incoherent pump and the effective gain is insufficient to overcome the cavity losses [10]. Thus, as the system undergoes self-quenching, the cavity fails to store lasing photons due to the presence of a strong incoherent pump and the photon field experiences strong fluctuations. Increasing cavity loss reduces the number of cavity photons and the two peaks in the Fano factor collapse to a single peak.

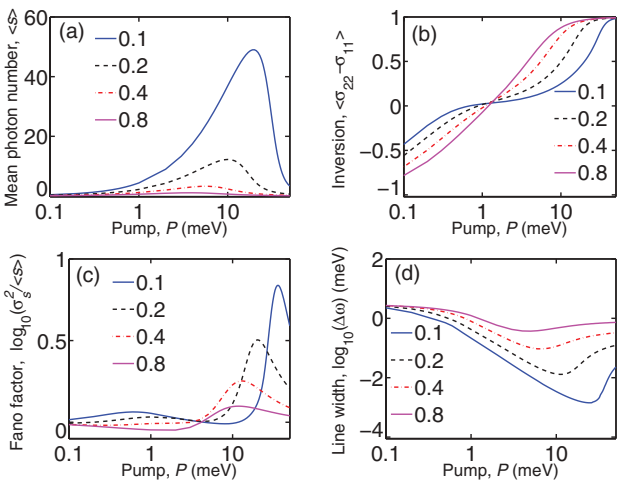

FIG. 2. (Color online) Variation of steady-state properties of a single two-level emitter coupled to a cavity field with incoherent pump rate, P, for the indicated values of cavity loss rate, κ (meV). (a) Mean photon number in lasing mode. (b) Inversion of emitter showing significant signature of inversion pinning for low optical loss, $\kappa = 0.1$ meV. (c) Fano factor for photon number, s. The laser threshold corresponds to a broad peak near $P = 1$ meV for $\kappa < 0.8$ meV. A peak due to self-quenching occurs for $P > 10$ meV. (d) Spectral linewidth. The pump axis is on a $\log_{10}$ scale. The dark solid line represents $\kappa = 0.1$ meV, the dotted line, $\kappa = 0.2$ meV, the dash-dotted line, $\kappa = 0.4$ meV, and the light solid line, $\kappa = 0.8$ meV. The parameters are $g = 1$ meV, $\gamma = 0.1$ meV, and $\omega = 1000$ meV.

A value of Fano factor or normalized second-order correlation $G^2(\tau = 0)$ less than unity signifies nonclassical light, which may exist when there is high cavity loss and low pump rate [12].

The inversion of the single emitter shown in Fig. 2(b) has a region of low slope in the presence of large photon number before it saturates completely. This is a signature of the carrier-pinning process that occurs in large conventional laser diodes when driven above threshold. However, in a single-emitter laser, the onset of self-quenching due to incoherent pumping destroys the coherence and reduces the effective gain. The system tries to compensate by increasing its inversion, fails, and dissipates energy by spontaneously emitting into modes other than the lasing mode.

As is characteristic of lasing behavior, the spectral linewidth of the photon field decreases with increasing number of cavity photons. The cavity with the lowest loss can attain the smallest linewidth. Far below threshold the linewidth is large because of the presence of a noninverted absorbing medium [10]. As shown in Fig. 2(d), the linewidth decreases with increasing number of cavity photons. As the system starts self-quenching, the linewidth increases, asymptotically approaching the empty cavity linewidth.

B. Multiple emitters

Results of our calculations shown in Fig. 3 confirm a previous suggestion [11] that adding emitters that act as independent sources coupled by the photon field is equivalent to making the cavity-emitter coupling, g, stronger. Enhanced coupling provides more emission into the lasing mode and self-quenching occurs at larger values of the pump rate. As more emitters are added the position of the two peaks in the Fano factor becomes more widely separated in pump rate. In Fig. 3 the steady-state behavior is plotted against the normalized pump rate (with the actual pump energy flowing into the system being obtained by multiplying the normalized value, P, by the number of emitters, N_e).

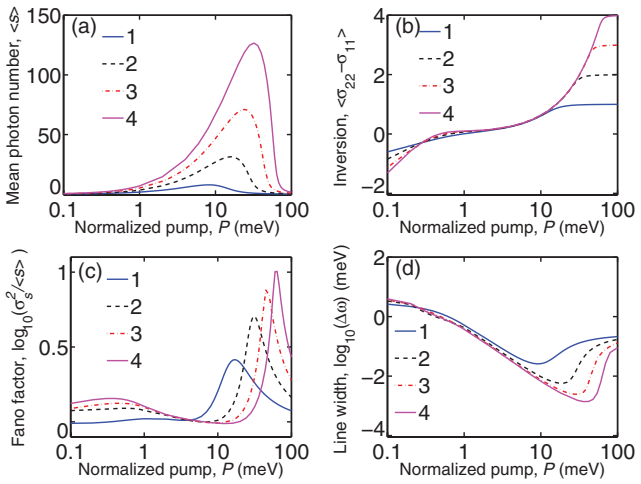

FIG. 3. (Color online) Variation of steady-state properties of multiple two-level emitters coupled to a cavity field as a function of normalized incoherent pump, P, for the indicated number of emitters. (a) Mean photon number in lasing mode. (b) Net inversion of emitters. (c) Fano factor. The laser threshold corresponds to a broad peak with $P < 1$ meV. The peak due to self-quenching occurs when $P > 10$ meV. (d) Spectral linewidth. The pump axis is on a $\log_{10}$ scale. The dark solid line represents $N_e = 1$, the dotted line, $N_e = 2$, the dash-dotted line, $N_e = 3$, and the light solid line, $N_e = 4$. The parameters are as in Fig. 2: $g = 1$ meV, $\gamma = 0.1$ meV, $\omega = 1000$ meV, and $\kappa = 0.25$ meV.

Due to a stronger effective coupling the peak that occurs at a smaller pump rate shifts to a lower pump rate with increasing number of emitters. Also, with increasing number of emitters, self-quenching occurs at higher values of normalized pump rate because photons generated by a given emitter induce transitions in other emitters. Similarly, for inversion, the device with the largest number of emitters has the strongest pinning.

C. Semiclassical rate equations derived from quantum master equations

We now compare the full quantum calculations with the steady-state values predicted by semiclassical rate equations. Here, the *semiclassical rate equations* are derived from the quantum master equations under an approximation in which correlations between emitter and photon operators are factorized. This factorization approximation is valid in the presence of large photon numbers.

For any system operator O, the equation governing its expectation value can be derived from the quantum master equation, [11]

$$\frac{d\langle O\rangle}{dt} = -\frac{i}{\hbar}\langle [O,H]\rangle + \mathrm{Tr}(OL\rho). \tag{22}$$

For system operators $s = a^\dagger a$, a, ${\sigma_k}^\dagger$, and σ_{zk}, the equations are as follows:

$$\frac{d\langle s\rangle}{dt} = -\frac{i}{\hbar}\sum_k g_k[\langle \sigma_k a^\dagger\rangle - \langle a{\sigma_k}^\dagger\rangle] - \kappa\langle s\rangle, \tag{23}$$

$$\frac{d\left\langle \sum_i \sigma_{zk}\right\rangle}{dt} = \frac{k}{\hbar}\sum_k 2g_k[\langle \sigma_k a^\dagger\rangle - \langle a{\sigma_k}^\dagger\rangle] - (\gamma + P)\sum_k\langle\sigma_{zk}\rangle + N_a(P-\gamma), \tag{24}$$

$$\frac{d\langle a\rangle}{dt} = -\frac{k}{\hbar}\sum_i g_k\langle\sigma_k\rangle - \frac{\kappa}{2}\langle a\rangle, \tag{25}$$

$$\frac{d\langle {\sigma_k}^\dagger\rangle}{dt} = -\frac{k}{\hbar}g_k\langle\sigma_{zk}a^\dagger\rangle - \frac{\gamma+P}{2}\langle{\sigma_k}^\dagger\rangle, \tag{26}$$

where σ_{zk} is the inversion of the kth emitter. Solving these equations and their complex conjugates in steady state yield mean cavity photon number $\langle s\rangle$ and net inversion above threshold $\langle\sum_k \sigma_{zk}\rangle$,

$$\langle s\rangle = \frac{1}{2\kappa}\left[N_a(P-\gamma) - \kappa\left(\frac{\hbar(\gamma+P)}{2g}\right)^2\right], \tag{27}$$

$$\left\langle\sum_k \sigma_{zk}\right\rangle = \frac{\hbar^2\kappa(\gamma+P)}{4g^2}. \tag{28}$$

As shown in the previous section, more emitters lead to more photons in the cavity and hence a better agreement is

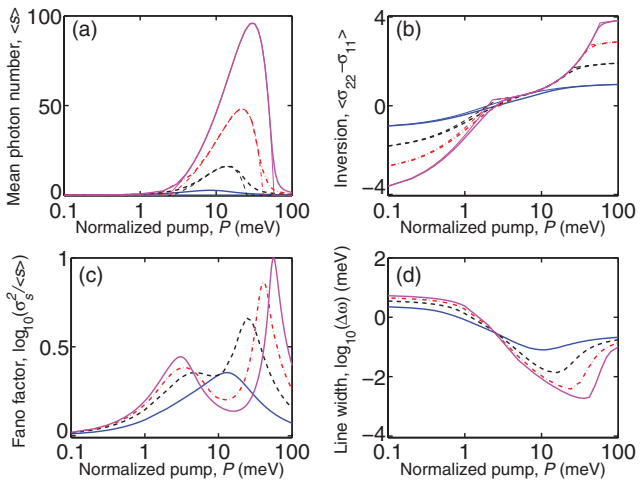

FIG. 4. (Color online) Comparison of steady-state properties derived from semiclassical rate equations and the full quantum theory. (a) Mean photon number in lasing mode. (b) Net inversion of emitters. (c) Fano factor. The threshold for $N_e \geqslant 2$ corresponds to a peak near $P = 3$ meV and the peak due to self-quenching occurs for $P > 20$ meV. (d) Spectral linewidth. The behavior for a different number of emitters is compared. The pump axis is on a $\log_{10}$ scale. The dark solid line represents $N_e = 1$, the dotted line, $N_e = 2$, the dash-dotted line, $N_e = 3$, and the light solid line, $N_e = 4$. The thicker lines denote quantum calculations and the corresponding thinner lines denote semiclassical calculations. The parameters are $g = 1$ meV, $\gamma = 2$ meV, $\omega = 1000$ meV, and $\kappa = 0.25$ meV.

observed with the semiclassical rate equation predictions. This is similar to increasing the cavity-emitter coupling, g, which also leads to more photons in the cavity.

The parameters in Fig. 4 are modified to produce a larger laser threshold compared to that shown in Fig. 3. This is done by enhancing the spontaneous emission rate γ into nonlasing modes. The cavity with a single emitter supports a single peak in the Fano factor. Increasing γ reduces the effective gain [10], which leads to a smaller number of photons in the lasing cavity.

There is good agreement between the predictions of the full quantum theory and the semi-classical rate equations in regions of large photon numbers as shown by Figs. 4(a) and 4(b). Disagreement is found near lasing threshold and self-quenching because the factorization approximation fails when average photon numbers are small.

D. Semiclassical master equations

It is interesting to compare the predictions of the full quantum calculations with those of the *semiclassical master equations* developed in Refs. [1,2]. Figure 5 shows transitions out of (n,s) in the n-s state space, where n denotes the discrete number of excited electronic states in the cavity and s denotes the number of photons. The trajectories of a biased random walk in the n-s state space are used to sample the solutions to the semiclassical master equations.

The random-walk calculations are modified in the sense that the number of emitters or excited states in the cavity is limited. Therefore, current can only pump the system if emitter excitation is possible. The semiclassical master equations account for energy and particle number conservation

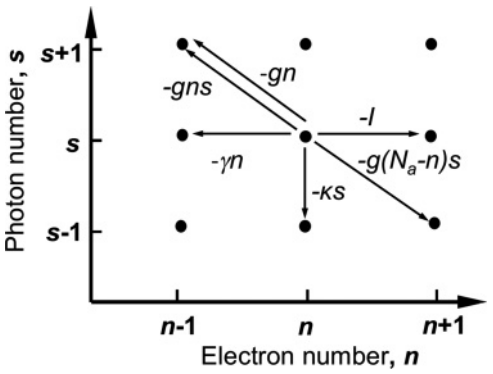

FIG. 5. Transition rates out of state (n,s). g is the dipole coupling constant, $-gns$ is the stimulated emission rate in the system at photon energy $\hbar\omega$, $-g(N_e - n)s$ is the stimulated absorption rate where N_e is the maximum number of emitters, γ is the spontaneous emission rate into modes other than the cavity mode, and κ is the total optical loss rate from the cavity. I is the excited-state injection (pump) rate.

but they do not include phase fluctuations and hence cannot reproduce the effects of self-quenching, which occur due to suppression of coherence. However, the method predicts the enhanced photon fluctuations around threshold quantified by the Fano factor, after which, with increasing pump rate, the excitation gets pinned and the cavity photon number increases. Figure 6 compares semiclassical master equation behavior with the full quantum model and shows good agreement near the threshold region before the onset of quenching. The net excitation is partially pinned at similar

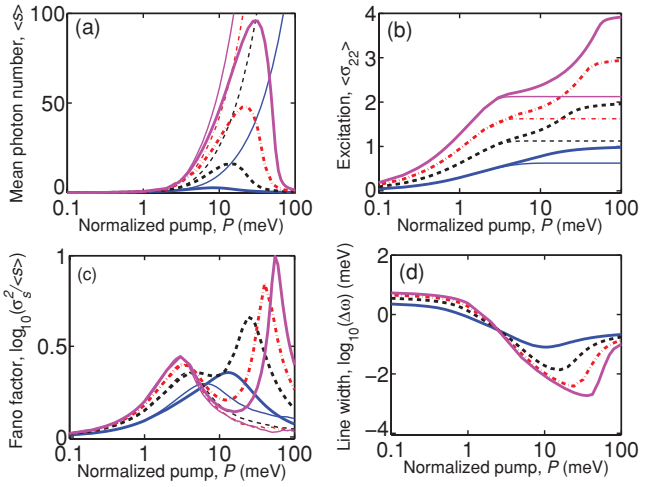

FIG. 6. (Color online) Comparison of steady-state properties derived from semiclassical master equations and the full quantum theory for different numbers of emitters. (a) Mean photon number in lasing mode. (b) Net inversion of emitters. (c) Fano factor. The laser threshold for $N_e \geqslant 2$ corresponds to a broad peak near $P = 3$ meV and self-quenching, which is a pure quantum effect, occurs for $P > 20$ meV. (d) Spectral linewidth. The pump axis is on a $\log_{10}$ scale. The dark solid line represents $N_e = 1$, the dotted line, $N_e = 2$, the dash-dotted line, $N_e = 3$, and the light solid line, $N_e = 4$. The thicker lines denote quantum calculations and the corresponding thinner lines denote semiclassical master equation calculations. The parameters are as in Fig. 4: $g = 1$ meV, $\gamma = 2$ meV, $\omega = 1000$ meV, and $\kappa = 0.25$ meV.

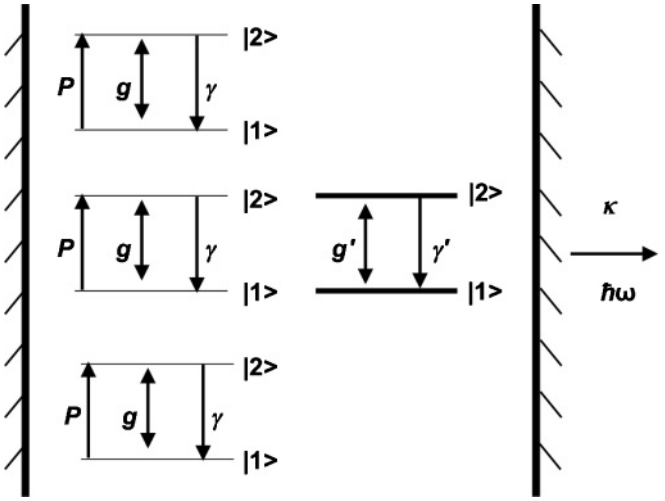

FIG. 7. System of multiple emitters coupled to a single optical cavity mode in the presence of a saturable absorber. The illustration is for $N_e = 3$ and $N_a = 1$. It is assumed that $g < g'$ and $\gamma < \gamma'$.

values of pump rate predicted by the semiclassical calculations [Fig. 6(b)]. The location of the lasing threshold pump rate, as determined by the first peak in the Fano factor, is also in close agreement with the semiclassical calculations [Fig. 6(c)]. These results validate the assumption that particle number quantization captures much of the full quantum model of multiemitter mesolasers [1,2] for pump rates below the onset of self-quenching. There is somewhat less agreement for the case of a single emitter, indicating that it is more sensitive to complete field quantization compared to the multiemitter case.

The semiclassical master equation predictions of lasing suppression around threshold and the associated excited electronic state depinning around threshold found in Refs. [1,2] are however absent in the full quantum model for N_e identical emitters. This is because, in a homogeneous quantum system, spontaneous emission into the lasing mode has the same coefficient as the net stimulated gain term in the presence of one photon [13–16]. The semiclassical master equation is not constrained in this way and the stimulated gain and spontaneous emission into the lasing mode are taken as independent phenomenological parameters [5,17,18]. The effects of lasing suppression around threshold and bimodal probability distributions may be captured in the full quantum model by including a saturable absorber in the system. This inhomogeneity provides an explanation of the origin of the phenomenological parameters used in the semiclassical master equation.

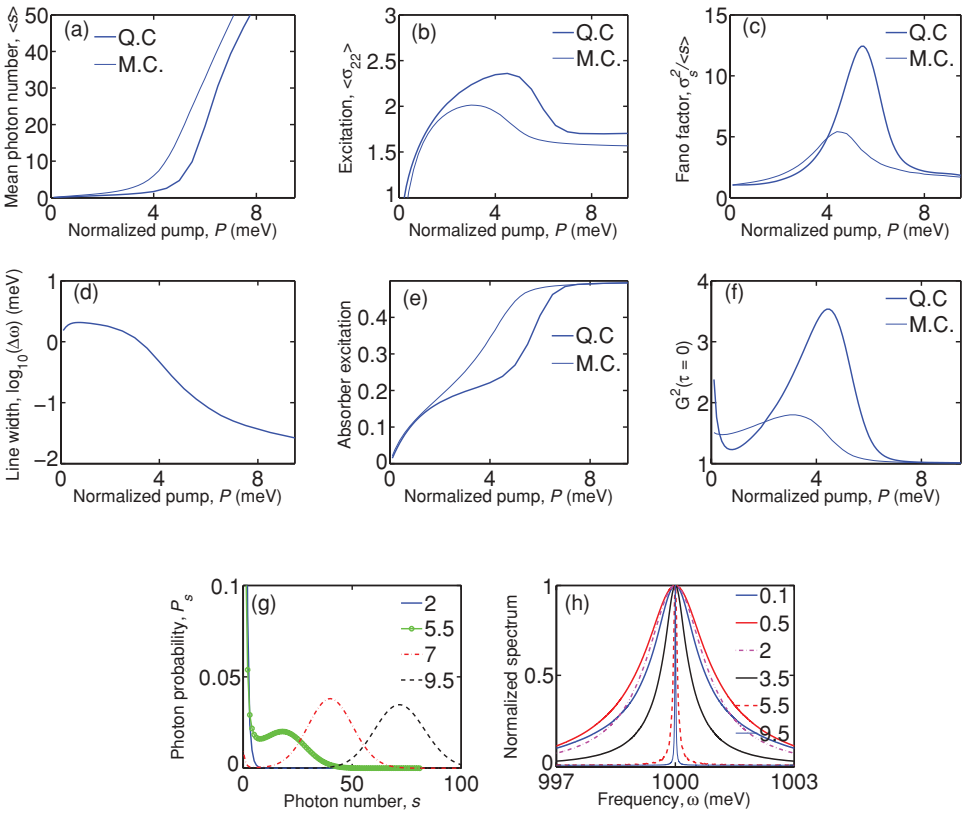

FIG. 8. (Color online) Steady-state properties of an emitter-photon system in the presence of a saturable absorber. Semiclassical master equation calculations [(MC), thin lines] and the full quantum theory calculations [(QC), thick lines] are shown. (a) Mean photon number in lasing mode. (b) Net excitation of emitters. (c) Fano factor. (d) Spectral linewidth. (e) Excitation of absorbing element. (f) Second-order coherence at zero delay, $G^2(\tau = 0)$. (g) Probability distributions across threshold from full quantum theory. (h) Spectrum at different normalized pump rates (meV). The emitter elements are $N_e = 3$; the absorbing element is $N_a = 1$. The parameters are $g = 1$ meV, $\gamma = 0.1$ meV, $\omega = 1000$ meV, $\kappa = 0.1$ meV, $g' = 4g$, and $\gamma' = 100\gamma$.

IV. SATURABLE ABSORBER

Inhomogeneity is incorporated in the quantum model of the laser by including a saturable absorber. As illustrated in Fig. 7, this is achieved by introducing N_a saturable absorber material elements, each coupled to the photon field by a coupling constant g' and decay rate γ'. This material is not incoherently pumped and it absorbs photons created in the cavity by emitters. Once saturated, the system may lase. The Hamiltonian is

$$H_S = \omega a^\dagger a + \sum_{k=1}^{N_e} \omega |2_k\rangle\langle 2_k| + g(\sigma_k a^\dagger + a\sigma_k{}^\dagger) + \sum_{k'=1}^{N_a} \omega |2_{k'}\rangle\langle 2_{k'}| + g'(\sigma_{k'} a^\dagger + a\sigma_{k'}{}^\dagger). \quad (29)$$

Including the interaction with reservoirs, the master equation is

$$\frac{d\rho}{dt} = \frac{i}{\hbar}[\rho, H_S] + \frac{\kappa}{2}(2a\rho a^\dagger - a^\dagger a\rho - \rho a^\dagger a) + \sum_{k=1}^{N_e} \frac{\gamma_k}{2}(2\sigma_k \rho \sigma_k{}^\dagger - \sigma_k{}^\dagger \sigma_k \rho - \rho \sigma_k{}^\dagger \sigma_k) + \sum_{k=1}^{N_e} \frac{P_k}{2}(2\sigma_k{}^\dagger \rho \sigma_k - \sigma_k \sigma_k{}^\dagger \rho - \rho \sigma_k \sigma_k{}^\dagger) + \sum_{k'=1}^{N_a} \frac{\gamma'_{k'}}{2}(2\sigma_{k'} \rho \sigma_{k'}{}^\dagger - \sigma_{k'}{}^\dagger \sigma_{k'} \rho - \rho \sigma_{k'}{}^\dagger \sigma_{k'}). \quad (30)$$

As shown in Figs. 8 and 9, with appropriate choice of parameters, results of the quantum model are similar to the predictions of semiclassical master equations. A linear scale is chosen in Fig. 8 for easy comparison with our previous results in Refs. [1,2]. The horizontal scale is limited to values of pump rate less than that at the onset of self-quenching. The behavior of a mesolaser with a saturable absorber for pump rates that include self-quenching is shown in Fig. 9.

Figures 8 and 9 show bimodal photon distributions [Fig. 8(g)] and excited-state depinning around threshold [Figs. 8(b) and 9(b)]. Emitter inversion (or excitation) depins around the lasing threshold to produce the extra photons required to saturate the absorber before the system can start lasing continuously, at which point the excitation gets pinned. The photon distribution near the depinned region is bimodal with a strong peak at zero photon number, indicating strong switching (or blinking) between the lasing and zero-photon states of the system. De-pinning also increases spontaneous emission into non-lasing modes.

The Fano factor shows a peak around the onset of lasing [Figs. 8(c) and 9(c)] and the linewidth decreases with increasing photon number [Figs. 8(d) and 9(d)], both of which are signatures of threshold behavior. With further increase of pump rate, the system enters its self-quenching behavior and the number of photons in the cavity decreases, the absorber loses its inversion, and the lasing emitters are pinned at the saturation value. The probability distributions in Fig. 8(g) from the quantum model show that the peak at $s = 0$ is reduced as the pump rate is increased. It reaches its smallest value

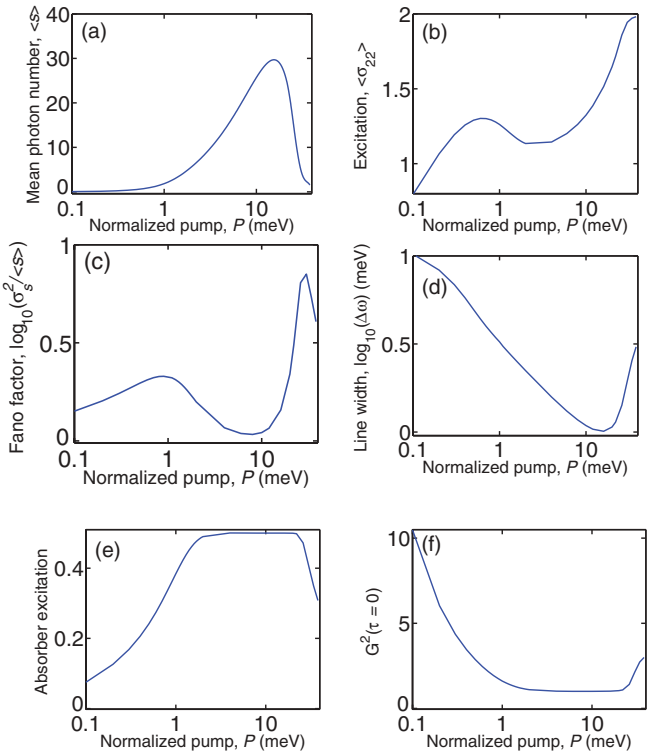

FIG. 9. (Color online) Steady-state properties of a two-emitter system in the presence of a saturable absorber. (a) Mean photon number in the lasing mode. (b) Net excitation of emitters. (c) Fano factor. The laser threshold corresponds to a broad peak near $P = 1$ meV and self-quenching corresponds to the peak near $P = 20$ meV. (d) Spectral linewidth. (e) Excitation of absorbing element. (f) Second-order coherence at zero delay, $G^2(\tau = 0)$. The number of emitter elements is $N_e = 2$ and the number of absorbing elements is $N_a = 1$. The pump axis is on a $\log_{10}$ scale. The parameters are $g = 1$ meV, $\gamma = 0.1$ meV, $\omega = 1000$ meV, $\kappa = 0.25$ meV, $g' = 4g$, and $\gamma' = 4\gamma$.

at a pump rate near the linear region of lasing, after which it again starts increasing because of the onset of quenching. The semiclassical behavior, however, loses this peak (at $s = 0$) and a single-peaked distribution remains and the system does not quench. The normalized second-order correlation $G^2(\tau = 0)$ increases in this region of bimodal distribution before it reaches a value of 1, showing a Poisson distribution as the system starts lasing.

With increase in photon number, the spectral linewidth shown in Fig. 8(d) initially *increases* before it starts decreasing. This is due to the presence of the absorber. Experiments with semiconductor quantum wire and quantum dot lasers whose active region is likely inhomogeneous also show an increase in spectral linewidth before a decrease with increasing pump around threshold [8,19]. At values of pump rate sufficiently large that the system quenches, calculations show that the linewidth is greater than that of the empty cavity. This occurs because absorber occupation is no longer inverted.

Figure 10 shows linewidth behavior with increasing pump rate below and near threshold for different absorber coupling strength, g'. The case with the smallest coupling, $g' = 1$,

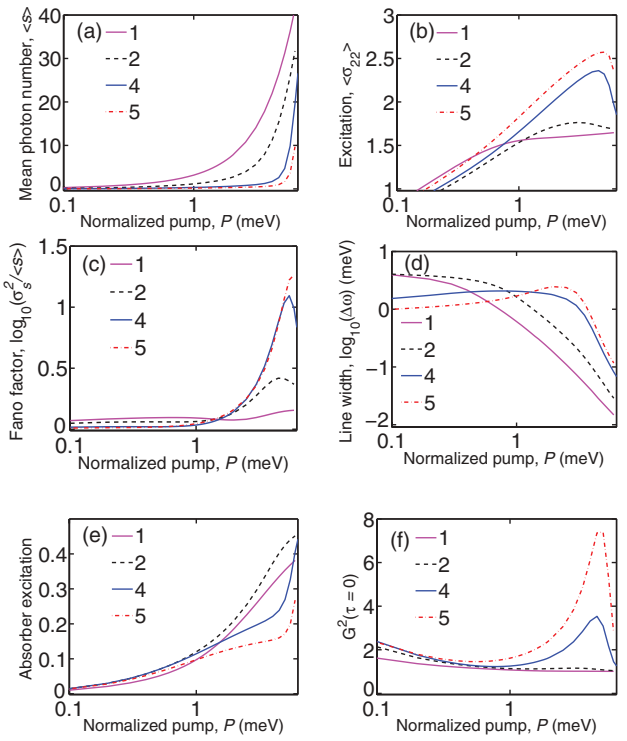

FIG. 10. (Color online) Comparison of steady-state properties of an emitter-photon system in the presence of a saturable absorber for indicated absorber coupling g' in meV. The normalized pump power is shown from low values up to values around threshold. (a) Mean photon number in the lasing mode. (b) Net excitation of emitters. (c) Fano factor. (d) Spectral linewidth. (e) Excitation of absorbing element. (f) Second-order coherence at zero delay, $G^2(\tau = 0)$. The number of emitter elements is $N_e = 3$ and the number of absorbing elements is $N_a = 1$. The pump axis is on a $\log_{10}$ scale. The parameters are $g = 1$ meV, $\gamma = 0.1$ meV, $\omega = 1000$ meV, $\kappa = 0.10$ meV, and $\gamma' = 100\gamma$. The curves correspond to different values of absorber coupling g' (meV).

behaves similar to a conventional laser. Figure 10(d) shows that increasing g' produces a greater broadening of linewidth or enhanced phase fluctuations in the region below threshold. The photon probability distributions are not bimodal in this region. However, at greater pump rates large values of g' create bimodal distributions and excitation depinning. This gives rise to a region of enhanced phase fluctuations and hence *increased linewidth*, before, with increased pump rate, experiencing enhanced amplitude fluctuations quantified by the Fano factor around threshold. Decreasing the value of γ' reduces the range of pump values over which linewidth increases.

Previous studies of lasers incorporating a saturable absorber, such as [20–23], make use of the large-particle-number approximation and (or) adiabatic elimination. This previous work contains some features common to our results, including lasing suppression and bimodal photon distribution near threshold. However, the previous work has no results for mesoscale laser excitation depinning or mesoscale laser spectral linewidth, and it is unable to predict quenching due to quantum decoherence.

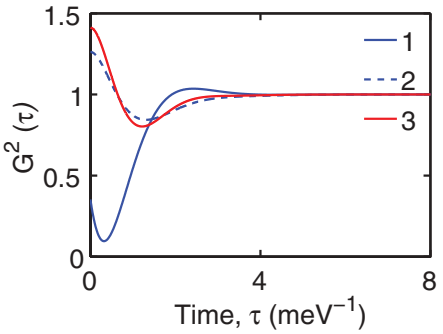

FIG. 11. (Color online) Time evolution of normalized second-order correlation $G^2(\tau)$ for the indicated number of emitters in the cavity. The parameters are $g = 1$ meV, $\gamma = 0.1$ meV, $\omega = 1000$ meV, and $\kappa = 2.5$ meV, and the normalized pump is $P = 0.5$ meV.

V. NONCLASSICAL LIGHT

As shown in Ref. [12], low pumping and high cavity losses lead to nonclassical states of light. The second-order correlation, $G^2(\tau = 0)$, at zero delay is used to identify nonclassical states. Figure 11 plots the variation of the normalized second-order correlation, $G^2(\tau)$, at $\tau > 0$ for one, two, and three emitters for high values of photon damping and low pump rates using Eq. (14). The one-emitter case shows nonclassical behavior as predicted because $G^2(\tau = 0)$ is less than 1. The time variation also violates Schwartz's inequality, $G^2(\tau) > G^2(\tau = 0)$ [3], and is a signature of antibunched behavior. Increasing the number of emitters removes this nonclassical behavior. For multiple emitters the correlation values at zero delay and the time variation are characteristic of bunched photon emission from a classical source [10,11,24,25].

VI. CONCLUSION

The fundamental contribution of field quantization to noise and fluctuations in mesoscale lasers that include inhomogeneity in the form of a saturable absorber has been investigated theoretically. Quantum fluctuations in this finite-sized dissipative system can influence spectral emission linewidth, suppress lasing, increase particle number fluctuations, and enhance spontaneous emission near threshold. We have presented numerical simulations of static and dynamic properties of mesoscale lasers using a quantum model with no special approximations (such as weak coupling between the field and reservoir or a single-atom emitter approximation). We have applied this model to an inhomogenous mesoscale laser containing N_e emitters and a saturable absorber and demonstrated existence of excitation depinning which has previously either been ignored or adiabatically eliminated. Our results provide an interpretation of empirically determined values of β used in semiclassical mesoscale laser models [18] as being due to the presence of an inhomogeneous medium and we have successfully established the connection between the semiclassical [1,2] and full quantum description of mesoscale lasers. Our work also provides insight into the role of phase and particle number fluctuations in determining the experimentally observed spectral and particle correlation behavior of small lasers [8,9,19].

Future work might explore the impact of quantum fluctuations in determining the temperature sensitivity of very small lasers and compare this with its known role in determining temperature dependence of conventional laser diodes [26–28].

ACKNOWLEDGMENTS

We acknowledge support by the National Science Foundation under Grant No. ECCS-0507270 and funding by DARPA.

[1] K. Roy-Choudhury, S. Haas, and A. F. J. Levi, Phys. Rev. Lett. **102**, 053902 (2009).
[2] K. Roy-Choudhury and A. F. J. Levi, Phys. Rev. A **81**(6), 013827 (2010).
[3] M. O. Scully and M. S. Zubairy, *Quantum Optics* (Cambridge University Press, Cambridge, UK, 1997).
[4] C. W. Gardiner, *Handbook of Stochastic Methods* (Springer-Verlag, Berlin, 1983).
[5] W. W. Chow and S. W. Koch, *Semiconductor-Laser Fundamentals* (Springer-Verlag, Berlin, Heidelberg, New York, 1999).
[6] H. Haken, in *Handbuch der Physik*, Vol. XXV/2c, edited by L. Genzel (Springer-Verlag, Berlin, 1970).
[7] W. H. Louisell, *Quantum Statistical Properties of Radiation* (Wiley, New York, 1973).
[8] M. Nomura, N. Kumagai, S. Iwamoto, Y. Ota, and Y. Arakawa, Nature Phys. Lett. **6**, 279 (2010).
[9] F. Dubin, C. Russo, H. G. Barros, A. Stute, C. Becher, P. O. Schmidt, and R. Blatt, Nature Phys. Lett. **6**, 350 (2010).
[10] O. Benson and Y. Yamamoto, Phys. Rev. A **59**, 4756 (1999).
[11] Y. Mu and C. M. Savage, Phys. Rev. A **46**, 5944 (1992).
[12] J. I. Perea, D. Porras, and C. Tejedor, Phys. Rev. B **70**, 115304 (2004).
[13] H. S. Ashour, M. Sokol, L. M. Pedrotti, and P. R. Rice, J. Opt. Soc. Am. B **24**, 8 (2007).
[14] C. W. Gardiner and A. Eschmann, Phys. Rev. A **51**, 4982 (1995).
[15] H. Haug and H. Haken, Z. Phys. **204**, 262 (1967); H. Haug, *ibid.* **200**, 57 (1967); **206**, 163 (1967).
[16] H. Haug, Phys. Rev. **184**, 338 (1969).
[17] A. F. J. Levi, *Applied Quantum Mechanics* (Cambridge University Press, Cambridge, UK, 2006).
[18] M. T. Hill *et al.*, Nature Photon. **1**, 589 (2007).
[19] K. Atlasov, M. Calic, F. Karlsson, P. Gallo, A. Rudra, B. Dwir, and E. Kapon, Opt. Express **17**, 18178 (2009).
[20] R. Roy, Phys. Rev. A **20**, 2093 (1979).
[21] L. A. Lugiato, P. Mandel, S. T. Dembinski, and A. Kossakowski, Phys. Rev. A **18**, 238 (1978).
[22] R. B. Schaefer and C. R. Willis, Phys. Rev. A **13**, 1874 (1976).
[23] J. O'Gorman, A. F. J. Levi, T. Tanbun-Ek, and R. A. Logan, Appl. Phys. Lett. **59**, 16 (1991).
[24] Y. M. Golubev and I. V. Sokolov, Zh. Eksp. Teor. Fiz. **87**, 408 (1984) [Sov. Phys. JETP **60**, 234 (1984)].
[25] H. Ritsch, P. Zoller, C. W. Gardiner, and D. F. Walls, Phys. Rev. A **44**, 3361 (1991).
[26] J. O'Gorman, A. F. J. Levi, S. Schmitt-Rink, T. Tanbun-Ek, D. L. Coblentz, and R. A. Logan, Appl. Phys. Lett. **60**, 157 (1992).
[27] J. O'Gorman, S. L. Chuang, and A. F. J. Levi, Appl. Phys. Lett. **62**, 1454 (1993).
[28] S. L. Chuang, J. O'Gorman, and A. F. J. Levi, IEEE J. Quantum Electron. **29**, 1631 (1993).